Vesicle motion and fusion is altered in chromaffin cells with increased SNARE cluster dynamics

Inmaculada López, Jose Antonio Ortiz, José Villanueva, Vanesa Torres, Cristina Torregrosa-Hetland, Maria del Mar Francés, Salvador Viniegra and Luis M. Gutiérrez*

Instituto de Neurociencias, Universidad Miguel Hernández-Consejo Superior de Investigaciones Científicas, Sant Joan d'Alacant, Alicante 03550, Spain.

* To whom correspondence should be addressed: Luis M. Gutiérrez, Instituto de Neurociencias, Universidad Miguel Hernández-CSIC, Sant Joan d'Alacant, Alicante 03550, Spain. Telephone: +34 965919562; Fax: +34 965919561; E-mail: luisguti@umh.es

Total characters: 60.003 (including spaces).

The expression of SNAP-25 fused to green fluorescent protein (GFP) has been instrumental in demonstrating SNARE role in exocytosis. The wild type GFP-SNAP-25 and a Δ9 form, product of Botulinum Neurotoxin A activity, the main ingredient in the BOTOX preparation, were employed here to study SNARE implication in vesicle mobility and fusion in cultured bovine chromaffin cells, a neuroendocrine exocytotic model. Using TIRFM, we have identified membrane microdomains of 500-600 nm diameter, that contain both SNAP-25 and syntaxin-1 and associate with synaptobrevin-II. Interestingly, while the SNAP-25 Δ9 formed similar clusters, they displayed increased mobility both laterally and in the axis perpendicular to the plasmalemma, and this correlates with the enhanced dynamics of associated chromaffin granules. SNARE cluster enhanced motion is reversed by elevation of the intracellular calcium level. Furthermore, single vesicle fusion was unlikely in the highly mobile vesicles present in the cells expressing SNAP-25 Δ9, which in addition, displayed in average slower fusion kinetics. Consequently, SNARE cluster dynamics is a new aspect to consider when determining the factors contributing to the mobility of the vesicles in close vicinity to the plasma membrane and also the probability of exocytosis of this granule population.

Key words; Chromaffin cells, vesicle motion, exocytosis, SNAP-25, membrane clusters, TIRFM**.**

Introduction

Exocytosis is a key event in the regulated release of neurotransmitters in neurons and neuroendocrine cells. The characterization of various proteins (SNAREs) that form the core complex involved in the specific docking and fusion of neurotransmitter-containing vesicles, has stimulated unprecedented progress towards elucidating the molecular bases of exocytosis [1-4]. The assembly of plasma membrane proteins (t-SNAREs) such as syntaxin [2] and SNAP-25 [5], as well as vesicle associated proteins (v-SNAREs) such as synaptobrevin II [6], provides the specificity required for vesicle docking and probably, the basic machinery for membrane fusion [7]. In addition to the use of classical tools such Clostridial neurotoxins [8], the generation of engineered SNARE constructs fused to the green fluorescent protein (GFP) has proven instrumental in defining the involvement of these proteins in specific steps of exocytosis. For instance, the use of a functional GFP-SNAP-25 chimera demonstrated the importance of specific amino acids in the C-terminal domain of this protein for core complex assembly and normal vesicle fusion in chromaffin cells, an accepted model of neuroendocrine exocytosis [9].

Subsequently, this and other constructs were employed to define the different stages of SNARE complex formation, its interaction with other proteins or factors, and the recruitment of different vesicle reservoirs [10-13]. Together, these studies demonstrated that ternary complex formation constitutes a late stage in membrane fusion. However, the chain of interactions between SNAREs and other proteins that controls this process (involving SNAPs, synaptotagmin, munc-18, etc) essentially remains undefined. In this sense, it has recently been established that syntaxin-1 and SNAP-25 associate to form a stable intermediate SNARE complex [14;15]. Moreover, these dimers cluster at the plasma membrane, defining

the active sites for exocytosis of dense granules in chromaffin cells [16].

In the present work, we have studied the existence of SNARE clusters in the plasma membrane of living chromaffin cells by over-expressing normal and altered forms of GFP and DsRred SNAP-25. Combining the use of these tools with total internal reflection fluorescent microscopy (TIRFM, [17;18]), a highly sensitive technique to resolve plasma membrane related events, has enabled us to produce a detailed description of how the manipulation of a SNARE protein alters the dynamic properties of the membrane patches formed by these proteins. More interestingly, the modification of the mobility of these patches is associated with the perturbation of chromaffin granule dynamics and also the probability of fusion.

Results

Native or altered forms of SNAP-25 fused to GFP form clusters in cultured bovine chromaffin cells.

This study was based on the expression of native and mutant SNAP-25 proteins in chromaffin cells with the aim of competing and eventually, substituting native SNAP-25 [9]. In addition, the SNAP-25a constructs utilized were coupled at their C-terminus to GFP to facilitate the visualization of the exogenously expressed protein [19]. This region of SNAP-25 was chosen for the fusion because it was less critical for protein function, permitting SNARE complex formation [20;21]. Two days after infection, bright green fluorescence could be detected in a high proportion of chromaffin cells, indicative of the expression of the GFP-SNAP-25 constructs. Inspecting the cells under TIRFM revealed the presence of round fluorescent patches, both in cells expressing the fusion protein containing the wild-type isoform (Fig. 1A) and in those expressing SNAP-25 lacking the last 9 C-terminal residues (GFP-SNAP-25 Δ9, Fig. 1B). This latter construct was designed on the basis of the cleavage of the same residues due to the inhibitory activity of BoNT A. The distribution of the size of the patches was similar with both constructs, with mean values of 0.25-0.26 μm^2 and modal values around 0.18-0.2 μm^2. These values indicate the presence of similar circular patches for both constructs with a mean diameter of 550-600 nm, slightly larger than the average chromaffin vesicle diameter (450 nm in our fluorescence measurements). Furthermore, both constructs were expressed at similar densities, around 0.12-0.14 clusters/μm^2. Since these measurements were similar to those obtained for syntaxin1/SNAP-25 plasma membrane microdomains in chromaffin cells [14] and in adrenal tissue [16], we assessed whether syntaxin1 was present in the cells expressing GFP-SNAP-25 constructs by immunostaining. The distribution of syntaxin1 matched perfectly that of GFP-SNAP-25 in our TIRFM images (Fig. 2 A and B)), reflected in the yellow color generated by superimposing the images (Fig. 2 C). Moreover, there was a high degree of colocalization, as it is shown in the colocalization mask depicting the pixels displaying more than 50 % of the fluorescence intensity in both channels (Fig. 2 D). When these images were visualized by confocal microscopy, 3D reconstruction depicted the patches at the periphery of the chromaffin cell spherical volume (see video 1 in Supplementary Material, use the repeat option of your video viewer when playing these videos). The SNAP-25 microdomains also contained synaptobrevin-2 in cells that co-

expressed GFP-synaptobrevin-2 and DsRed-SNAP-25 (Fig. 2 E to H). An estimation of the colocalization pixels with more than 50 % of the labeling in both channels revealed that SNAP-25 patches colocalized with 67±8 % of the syntaxin-1 and 59±7 % of the synaptobrevin II labeling (determinations performed in 10 cells). To demonstrate that these SNARE clusters are located indeed in the plasma membrane of the cells expressing the GFP-SNAP-25 constructs we conceived experiments labeling the exocytotic sites by antibodies against dopamine-β-hydroxylase incorporated into the plasmalemma after exocytosis. Confocal images of GFP-SNAP-25 and exocytotic sites show the disposition of both labelings in the same plane of the cell periphery (Figure 1, Supplementary Material).These experiments demonstrated that the SNAP-25 constructs form patches in the plasma membrane of cultured chromaffin cells and that these microdomains also contain syntaxin-1, as well as interacting with the GFP-synaptobrevin-2 present in chromaffin vesicles [21]. In addition the presence of the endogenous SNAP-25 protein was analyzed using polyclonal anti-SNAP-25 antibodies in cells expressing both GFP-SNAP-25 constructs. As can be observed in the Supplemental Fig. 2, most of the clusters detected with the SNAP-25 antibodies present a strong GFP labeling and in average, less that 10 % of the clusters present much lower levels of GFP-SNAP-25 or GFP-SNAP-25 Δ9, therefore the over-expressed proteins seems to be abundant in the vast majority of the clusters.

SNARE microdomains formed by GFP-SNAP-25 and GFP-SNAP-25 Δ 9 display different mobility.

The morphological parameters of the microdomains formed by the wild type and the Δ9 GFP-SNAP-25 constructs are very similar. However, time lapse studies taken at 1 s intervals during 1 min periods, revealed that they display quite different mobility (see the behavior of the microdomains depicted in Fig 3 A and B and the clearly different dynamics visualized in video 2 -GFP-SNAP-25 wild type, 6 times accelerated- and video 3 -GFP-SNAP-25 Δ9-. in the Supplementary Material). GFP-SNAP-25 microdomains displayed limited movement characterized by short range oscillations in the XY plane and a very stable average ROI intensity during the period of observation, indicative of restricted mobility in the Z plane in TIRFM images (Fig. 3 C and D). In contrast, patches of the truncated form moved more freely in the XY plane and displayed more pronounced oscillations, suffering less restriction to their movement in the Z axis. An analysis of microdomain mobility by tracking the centroids corresponding to the patches observed showed the differences in the velocities between these two forms of SNAP-25 (Fig. 4 A). Wild type SNAP-25 presented a relatively narrow distribution of velocities that fits well to a Gaussian model centered on the modal value of 20 nm/s and with a mean average speed of 22 ± 1 nm/s. Alternatively, the GFP-SNAP-25 Δ9 patches displayed a wider distribution centered on a modal Gaussian value of 32 nm/s and with a mean average speed of 36 ± 3 nm/s. This analysis also indicated that 25-30 % of the microdomains formed by the truncated construct were more mobile than any of the patches formed by the wild type construct. The mean square displacement (MSD) was also analyzed at different time intervals and these values were averaged to generate the MSD vs time plot (Fig. 4

B). Assuming that patch movement is governed by a single diffusion coefficient, its value can be derived from the fitted slope (slope=4xD: [22]). Thus, the diffusion coefficient was calculated as 4.6 $\pm$ 0.1 $x10^{-5}$ $\mu m^2/s$ for GFP-SNAP-25 microdomains (n=74 patches from 29 cells), whereas the theoretical diffusion coefficient was estimated to be 12.0 $\pm$ 0.1 $x10^{-5}$ $\mu m^2/s$ for the GFP-SNAP-25 Δ9 construct (n=99 patches from 33 cells). This value was twice that of the characteristic diffusion coefficient for the patches in cells expressing the wild type form of SNAP-25.

Further evidence of this change in the mobility of the SNARE patches was obtained from the study of their motion in the Z plane. The maximum fluorescence intensity corresponding to the pixels defining SNARE patches were studied (72 patches for both constructs during 60 s taken at 1 s intervals), and then these fluorescence intensities were transformed into z distances using the equation defining the exponential evanescent field decay. The z distances were calculated for 3 representative patches containing either construct during 1 min period (Fig. 5A). As observed the brilliant patches of GFP-SNAP-25 wild type tend to move in distances ranging from 50 to 100 nm on the glass coverslip where the evanescent field is originated. In contrast, the GFP-SNAP-25 Δ9 patches moved further and were generally spread over a wider range, covering distances from 150 to 300 nm. The fraction of time individual granules spent at different distances from the origin of the evanescent field was estimated and plotted as a distribution (Fig. 5B). While the patches formed by wild type SNAP-25 presented an average oscillation with a maximum probability of finding them at the modal Gaussian value of 80 nm (average mean value of 128 ± 9 nm, n=74 patches), the GFP-SNAP-25 Δ9 patches presented a maximal probability of being locating at about 150 nm (average mean distance of 197 ± 14 nm, n=72 patches). The amplitude of movement could be calculated for each individual patch (Δz) during the experimental observation time of 1 min. These Δz values could be binned (20 nm step size) and analyzed as distributions for the values corresponding to both GFP-SNAP-25 constructs. Accordingly, the magnitude of these changes are clearly greater for the Δ9 truncated construct when compared with the z increments found for the wild type patches (Fig. 5C and D). On average, the mean mobility range was found to be 107 ± 7 nm for the wild type patches versus 150 ± 9 nm for the patches formed by the truncated isoform. Taking together the results obtained regarding both XY and Z movement, it was clear that the patches formed by the truncated form of SNAP-25 are subjected to less restricted movement. Thus, they tend to be located further from the cell limits and hence, the exocytotic sites in the plasmalemma. In these studies we found no significant correlation between the level of expression (maximum of fluorescence for every patch) and the patch mobility.

SNARE cluster enhanced motion in cells expressing the truncated form is abolished by high $[Ca^{2+}]_i$

Is SNARE microdomain behaviour linked to the molecular properties of SNAP-25 regarding core complex formation?. To answer this question, we conceived an experiment based in the seminal observation that in cells treated with BoNT A, high levels of intracellular calcium promotes synaptotagmin binding to the SNAP-25 forming part of the complex overcoming the toxin effects [23]. Cells expressing GFP-SNAP-25 Δ9

were incubated in a médium containing 10 mM calcium in the presence of the calcium ionophore ionomycin (5 μM, 5 min), time-lapse studies of cluster mobility was performed before and after cell treatment. Figure 6 shows that the mobility of the SNARE clusters characteristic of the truncated form expression were affected by this manipulation increasing intracellular calcium levels. The study performed in 79 patches from 30 cells proved for example that the average speed of 36 ± 1 nm/s and the coefficient of diffusion of 12.1 ± 0.3 $x10^{-5}$ $\mu m^2/s$ changed to 25 ± 1 nm/s and 4.3 ± 0.1 $x10^{-5}$ $\mu m^2/s$, respectively (Fig. 6 C and D). In addition the clusters become brighter indicating the approximation to the origin of the evanescent field and ΔZ changed from 148 ± 7 nm to 74 ± 8 nm (n=73 patches). Thus, both, lateral and Z motion parameters changed to values that were characteristic of the clusters containing the wild type form. As an additional control, we have found that GFP-SNAP-25 clusters do not change significantly their motion after the elevation of intracellular calcium (Fig. 6 E and F, average speed of 28 ± 2 nm/s and the coefficient of diffusion of 3.7 ± 0.6 $x10^{-5}$ $\mu m^2/s$, n=65 patches).

Vesicle motion is correlated with the mobility of SNARE patches.

To address how the behavior of SNARE microdomains influence vesicle motion, we labeled chromaffin granules with the acidophilic dye lysotracker red in cells expressing the GFP-SNAP-25 constructs [24]. TIRFM was used to first visualize the position of the GFP-SNAP-25 microdomains (Figure 7A), and then the laser and critical angle was changed to visualize the vesicles (Figure 7B) and to analyze the motion of the vesicles that colocalized with the SNARE patches (Figure 7C and D). Accordingly, we ensured that the vesicles studied were associated with SNARE clusters where the exogenous GFP-SNAP-25 was present. The velocity distribution histogram and the analysis of MSD vs interval time plots revealed a strict relationship between the movement of the SNARE cluster and the mobility of the associated granules. Granules associated with the wild type SNAP-25 isoform moved with an average speed of 23 ± 1 nm/s and the apparent coefficient of diffusion was estimated as 3.7 ± 0.2 $x10^{-5}$ $\mu m^2/s$ (n= 64 vesicles from 10 cells), approaching the values obtained for the movement of SNARE microdomains. More interestingly, the vesicles associate with SNARE clusters comprised of the truncated Δ9 form of SNAP-25 (Figure 7E to H) displayed more rapid lateral motion, reaching an average speed of 30 ± 1 nm/s and a diffusion coefficient of 15.0 ± 0.1 $x10^{-5}$ $\mu m^2/s$ (n=57 granules from 10 cells). Furthermore, the vesicles associated with the SNARE microdomains containing truncated SNAP-25 were preferentially localized further away from the plasma membrane in the z plane (Fig. 7K), displaying a significantly enhanced amplitude of z movement (Fig 7, L). Thus, considering the parameters obtained for lateral movement and that in the z plane, as well as the shape of the corresponding distributions, the mobility of the chromaffin vesicles in the proximity of the plasma membrane was strictly related to the dynamic characteristics of the SNARE clusters associated with the granules. These conclusions were obtained from independent measurements of SNARE cluster and vesicle dynamics, and since different laser wavelengths were used there can not be influenced by fluorescence cross-talk. Furthermore, the colocalization of DsRed-SNAP-25 and lysotracker green vesicles labeling over

time in experiments performed using single laser illumination under TIRFM and with simultaneous acquisition further supported the conclusions, particularly given that the critic TIRFM angle is fixed (see Supplementary Material Figure 3). In order to discard any influence of GFP-SNAP-25 overexpression artifacts we performed additional control experiments with cells expressing GFP-synaptobrevin with or without cotransfection with the light chain of BoNT A. The TIRFM analysis of the motion of the vesicles containing the labeled synaptobrevin shows that after the expression of the toxin for 24 h, both the average vesicle speed and the apparent coefficient of diffusion derived from MSD curves increased doubling that obtained in control cells in the absence of toxin expression (see Supplementary Material Figure 4). Thus, these experiments proved that the truncation of wild type SNAP-25 with the light chain of BoNT A reproduced the vesicle behavior obtained with overexpression of GFP-SNAP-25 Δ9.

Highly mobile granules in cells expressing SNAP-25 Δ9 display a low probability of exocytosis.

In order to study the impact of the changes observed in SNARE and vesicle movement on the secretory process, TIRFM was performed to correlate vesicle motion with the fusion process. Such experiments required the expression of DsRed-SNAP-25 constructs and incubation with 2 μM acridine orange, a dye accumulates in the granule matrix and produces an increase in green fluorescence upon neutralization during exocytosis. It is important to note that acridine orange accumulated in acidic matured granules also produces an emission of red fluorescence that could also be used to visualize the vesicle population. Both, DsRed and acridine orange are excited with the same 488 nm laser and therefore, we can simultaneously assess the presence of vesicles/SNARE (red fluorescence, left side of images and videos) and exocytotic fusion (flashes of green fluorescence, right side) using an emission splitter (as seen in Fig. 8 and the corresponding video 4 and video 5 of Supplementary material).

The cells expressing strong red fluorescence of DsRed-SNAP-25 expression (Fig. 8A) were subjected to depolarizing stimuli (KCl 59 mM) for 1 min and the number of fusing granules were calculated from the accumulative average images of the green emission channel (Fig. 8C). The percentage of fused vesicles was estimated and in cells expressing wild type DsRed-SNAP-25, 76 ± 4 % of the vesicles visualized in TIRFM fused during a 1 min stimulus (Fig. 8E, 515 fusions observed from the 700 vesicles studied). The red emission images (see video 4) demonstrated that these granules presented very limited movement, characteristic of the wild type form of SNAP-25. When the cells expressed the Δ9 truncated SNAP-25, granule movement evidently increased (see video 5) but fewer vesicles fused during the prolonged 1 min depolarization (Fig. 8B and D, 434 fusions of the 1029 vesicles studied in 19 cells). While these experiments represented the average of many cells, they resulted in an estimated 42 ± 6 % of fusion during a 1 min stimulation, almost half of that estimated for control cells expressing the wild type form (Fig. 8 E). Moreover, even in cells infected with the amplicons expressing the truncated form of SNAP-25, most of the granules that fuse present relatively little movement compared with the granules that display higher mobility and that rarely exocytose. In fact, we have estimated that 19 % of the vesicles present high mobility,

moving more than 2 vesicle diameters in 20 s (191 vesicles from 1029 studied) and only an 8 % of these vesicles fused (Fig. 8 F). In the same cells expressing the truncated Δ9 form of SNAP-25, the rest of the vesicles (81 %) present low mobility and higher probability of fusion (50 ± 5 %, n=19 cells). Thus, the probability of fusion of the vesicles presenting high mobility is significantly lower ($p<0.0001$) than the corresponding to the relatively immobile vesicles (Fig. 8 F). The images of granule fusions at 20 ms intervals could be used to study the overall level of secretion, and the maximal fluorescence in the green channel could be plotted versus time to produce a secretory profile with individual exocytotic events as spikes (Fig. 8G). A simple inspection of the two profiles revealed the diminished probability of fusion found for the cells expressing the truncated isoform of SNAP-25.

Vesicle fusion is slower in chromaffin cells expressing more mobile SNARE microdomains.

Interestingly, well resolved optical spikes that resemble amperometric fusion events could be used to analyze the individual fusion kinetics. Indeed, the time course of the green flashes were parallel to vesicle disappearance by exocytotic fusion (visualized in the red channel), as can be observed for the granules of control and truncated SNAP-25 expressing cells (Fig. 9A and B). These fusion spikes could then be analyzed in order to obtain the kinetic properties of such fusion events, obtaining parameters such the time at the half height ($t_{1/2}$) that revealed the speed of release. When hundreds of such events were studied in cells expressing the wild type form of SNAP-25, it was evident that the fusion characteristics were relatively homogeneous, with $t_{1/2}$ distributions centered on a modal value of around 120 ms and an average value of 178 ± 7 ms. (n=370 vesicles from 22 cells, Fig. 9G). Thus, the most frequent spike in cells expressing the wild type form of SNAP-25 is relatively narrow (see Fig. 9E), indicating that the release of the acridine orange from the granules in less than 500 ms in this optical measurement (see the average spike in Fig. 9F). When the fusion spikes of the cells expressing GFP-SNAP-25 Δ9 were analyzed, the distribution revealed a $t_{1/2}$ modal value of 160 ms with a mean value of 218 ± 9 ms (n=342 fusions from 29 cells), representing a relatively small but statistically significant increase of 22 % from the control values ($p<0.001$, Fig. 9H). Thus, the most frequent and average fusion spikes from cells expressing the truncated form revealed slower kinetics than the control fusion events obtained in cells expressing the wild type isoform (Fig. 9F). Moreover, even in cells infected with the amplicons expressing the truncated form of SNAP-25, most of the granules that fuse present relatively little movement compared with the granules that display higher mobility and that rarely exocytose. In fact, we only detected 4 fusions in the more mobile granules from the 342 vesicle fusions analyzed. These granules displayed oscillations in fluorescence considered as high mobility in the Z axis prior to fusion (as observed in Fig. 9E).

Discussion

Present data indicate that the mobility of the SNARE complexes influences the movement of the associated vesicles located in the proximity of the plasmalemma. We found also that expression of the Δ9 truncated form of SNAP-25 produced formation of highly mobile patches and reduced the probability of fusion of the associated granules. This

is in keeping with the effects of Botulinum Neurotoxin A which cleaves SNAP-25 and yields a product identical to Δ9 construct, therefore our experiments proved that the product of toxin action targeted their cellular partners.

SNAREs form dynamic microdomains when expressed in neuroendocrine chromaffin cells

We found that GFP-SNAP-25 forms round clusters that are associated with syntaxin-1 and that also interact with GFP-synaptobrevin II. These clusters are present at the cell contour in equatorial confocal images and they have an average diameter of 500-600 nm, in agreement with the size of SNARE microdomains in cultured chromaffin cells [14] and intact adrenal tissue [16] . The relatively high fluorescence intensity and the absence of decay catastrophe (all or non decay of fluorescence) seem to be incompatible with these being individual SNARE molecules. Membrane associated clusters of SNAREs have also been reported in other secretory systems such PC12 [25] and MIN6 beta cells [26]. It is important to notice that the reported size for these clusters in confocal or TIRFM based studies are clearly overestimated, in this sense the resolution improvement of STED microscopy has allowed the estimation of syntaxin-1 clusters in PC12 cells, being 70-90 nm is diameter, 5-6 times lower than the estimated by confocal microscopy [27]. Furthermore, TIRFM imaging reveals that the dynamics of such clusters correspond to relatively immobile patches when considering the wild-type GFP-or DsRed SNAP-25. Indeed, the modal speed of 20 nm/s corresponded to the linear displacement of one patch diameter in 30 s. Since the movement reverses direction continuously, the "normal" patch rarely moves further than one diameter during the experimental period of minutes. This restricted movement changes significantly when considering the truncated Δ9 SNAP-25 isoform, increasing the average speed by about 50 % and by two-fold the apparent diffusion coefficient. This enhancement of SNARE cluster kinetics could be appreciated in the accelerated videos provided here. Moreover, the narrow evanescent field of excitation in TIRFM (around 200 nm) is particularly sensitive to the movement in the Z plane of such clusters. While the wild-type clusters moved over distances of around 80-100 nm, the modal value for GFP-SNAP-25 Δ9 clusters was around 150 nm. Interestingly, the range of Z movement (ΔZ) displayed a significant increase in the amplitude of Z motion for the truncated isoform of SNAP-25. Interestingly, intracellular calcium elevation changes the motion of these highly mobile patches to the more restricted motion characteristic of the microdomains formed by the wild-type form of SNAP-25. Since, it has been proven that high calcium promotes synaptotagmin binding to the C-terminus of SNAP-25 forming part of SNARE complexes in cells treated with BoNT A [23]. These experiments along with the prior demonstration of the formation of ternary SNARE complexes with diminished thermostability by SNAP-25 Δ9 [21], support the notion that this truncated isoform contributes to labile SNARE complexes with an open conformation [10]. Such a conformation would favour a wider amplitude of movement as detected in our TIRFM experiments, but elevated calcium will drive the formation of productive tight complexes with its characteristic cluster low motion.

The motion of chromaffin granules is correlated with SNARE microdomain dynamics

An important consequence of the formation of SNARE complexes with different biochemical and dynamic properties is the alteration of the movement of vesicles in the immediate vicinity of the plasma membrane. This was evident through the analysis of the movement of the vesicles that colocalize with SNARE patches in the XY and Z planes. This is the first direct demonstration of how a labile GFP-SNARE construct affects the movement of the docked or tethered vesicles located close to the membrane. This observation accounts for the change in the rate and range of lateral movement of granules in chromaffin cells expressing the light chain of BoNT A as presented here or cells treated with the full toxin [28]. It also clarifies the shorter residence time of the vesicles closely apposed to the plasmalemma in cells expressing the neurotoxin [29]. Our results support the idea that t-SNAREs strongly influence the tethered state of the vesicles, initially identified in mouse embryonic chromaffin cells lacking the syntaxin-1 binding modulator Munc18-1 [30]. Two models of tethering have been proposed on the basis of these data. While the first implies the possibility of an initial docking to a Munc-18/syntaxin 1 platform and a posterior interaction with SNAP-25, the second model implies the formation of syntaxin 1/SNAP-25 dimers in which Munc-18 facilitates posterior binding to v-SNAREs. Our results favor the latter model, since syntaxin-1 is present in the dynamic SNAP-25 clusters and these microdomains pre-exist and define the sites for vesicle fusion [16]. In addition our results are in agreement with the recent demonstration that the primed and docked states could be distinguished by the mobility of the vesicles [31], while we move further by proving the direct implication of SNAREs through the change in the mobility of their clusters linking the vesicles with the plasma membrane.

Exocytosis is impaired in highly mobile SNARE microdomains comprised of SNAP-25 Δ9.

Our experimental approach using TIRFM allowed us to analyze also how the change in the dynamic properties of SNARE clusters influences fusion kinetics. In doing so, we also developed a new approach to analyze fusion kinetics based on the increase of green fluorescence after acridine orange neutralization during exocytosis, a methodology that is an optical simile of the amperometrical detection of catecholamines. The most striking finding was the low probability of fusion observed for highly mobile vesicles that constitute 33% of the granules present in the cells expressing the truncated SNAP-25 construct. When we analyzed the total fusion of vesicles with different mobility's, the probability of fusion in a cell expressing the truncated form was a half that in cells expressing the wild type form. Indeed, fusion of a highly mobile vesicle was a rare event, and we only found 4 fusions from 342 analyzed events in cells expressing SNAP-25 Δ9. Therefore even in the cells presenting an elevated number of highly mobile vesicles, the probability of fusion of these vesicles was estimated to be around 3-4 %, and most of the fusion observed came from relatively "normal" immobile vesicles. However, this truncation had a relatively minor effect on the fusion kinetics, which was only slightly slower than those in control cells. This effect is relevant since SNAP-25 is thought to participate in the modulation of fusion pore kinetics. This is

important to define the exact role of SNAREs as part of the fusion machinery [7]. However, this issue is controversial since this role is supported by some studies based on amperometric measurements [9;21], while no relevant changes in fusion kinetics were found in others [32;33]. To solve this question further study of the fusion pore behaviour in cells where the native protein is absent will be instrumental. Nevertheless, the present work clearly establishes that altered forms of SNAREs give rise to the formation of clusters with differential kinetic properties, altering the coupling of vesicles to the plasma membrane and therefore, the mobility of the docked or tethered vesicles. In addition this experimental manipulation significantly affects the probability of fusion of these highly mobile granules. The possibility of visualizing SNARE clusters, associated vesicles and the fusion process itself represents an opportunity to study not only the associated dynamics of the elements constituting the secretory machinery, but also the interaction of these elements with other factors, such as docking and tethering proteins that comprise the actives sites for exocytosis (i.e., cytoskeleton).

Materials and Methods

Chromaffin cell preparation and culture.

Chromaffin cells were isolated from bovine adrenal glands by collagenase digestion and they were further separated from the debris and erythrocytes by centrifugation on Percoll gradients as described elsewhere [34]. The cells were maintained as monolayer cultures in Dulbecco´s modified Eagle´s medium (DMEM) supplemented with 10 % fetal calf serum, 10 μM cytosine arabinoside, 10 μM 5-fluoro-2`-deoxyuridine, 50 IU/ml penicillin and 50 μg/ml streptomycin. The cells were harvested at a density of 150,000 cells/cm^2 in 35 mm-Petri dishes (Costar), and they were used between the third and sixth day after plating.

Generation of GFP and DsRed constructs with SNAP-25 and synaptobrevin, and cell infection.

The pEGFP-C3 and pDsRed-C3 expression vectors (Clontech, Palo Alto, CA) encode a red-shifted variant of wild-type GFP and RFP respectively [35]. The cDNA corresponding to the SNAP-25a isoform [19] was cloned into the XhoI and BamHI sites of pEGFP-C3 and pDsRed-C3 to express this protein fused in-frame at the C-terminus to EGFP (construct GFP-SNAP-25) and DsRed (construct DsRed-SNAP-25) respectively. The Δ9 deletion was generated by PCR of a fragment corresponding to the C-terminus of SNAP-25, using the GFP-SNAP-25 construct as template and a sense primer that corresponds to amino acids 80-86 of SNAP-25 (5'-AGATTTAGGGAAATGCTGTGG-3'). The amplified DNA carried an internal HindIII site, close to the 5'-end, and the previously mentioned BamHI site at the 3'-end. These enzymes were used to substitute the original SNAP-25 sequence by the modified one in the EGFP-SNAP-25 and DsRed-SNAP-25 vectors.

To produce an N terminal in-frame fusion of synaptobrevin with EGFP or DsRed, the coding region corresponding to synaptobrevin II was amplified by PCR with the following primers: 5'-GCCGAATTCCCGCCATGTCGGCTAC C-3' (sense) and 5'-GCCGGATCCGAGC-TGAAGTA-AACGATGATG -3' (antisense). The PCR product was digested with *Eco*RI and *Bam*HI and cloned into the same sites of the pEGFP-N1 and pDsRed-N1 expression vectors.

The constructs were transferred from the pEGFP-C3/N1 or pDsRed-C3/N1 vectors to the pHSVpUC vector [36] and primary cultures of chromaffin cells were infected with the Herpes Simplex virus (HSV-1) amplicon containing these constructs. The packaging of the different helper viruses (HSV-1 IE2 deletion mutant 5dl 1.2) was carried out as described previously [37]. The viral infection efficiency was determined by fluorescent microscopy using serial dilutions of the purified virus. The dilution producing 20-40% infection efficiency (usually 20-40 μl virus per 35 mm-plate containing 1 ml of medium) was chosen for the subsequent experiments. EGFP and DsRed fluorescence was observed one day after infection and it persisted for at least two days.

In some control experiments we performed simultaneous transfection of chromaffin cells with GFP-synaptobrevin II and the light chain of BoNT A [38] using an Amaxa kit for primary mammalian neural cells (Amaxa Inc. Gaithersburg, MD, USA).

Confocal microscopy studies of the cellular distribution of SNAP-25 and syntaxin 1.

Cells expressing GFP-SNAP-25 constructs were fixed and permeabilized using a modification [39] of the method described by Lazarides [40]. Briefly, cells were fixed with 4 % paraformaldehyde (PFA) in phosphate buffered saline solution (PBS) for 20 min. The cells were then permeabilized with 0.2 % Triton X-100 in 3.6 % formaldehyde for 10 min and washed twice for 10 min with 1% bovine serum albumin (BSA) in PBS. Labeling of syntaxin-1 was performed overnight in PBS + 3% BSA containing a 1:200 dilution of chicken antibodies raised against recombinant rat syntaxin1A. After extensive washes, a secondary TRICT-coupled rabbit anti-chicken antibody (1:200 dilution, Sigma, Madrid, Spain) was added and after 2 h, the unbound material was washed away with PBS. In some experiments, anti-dopamine β-hydroxylase antibodies were employed as described elsewhere [16] to determine exocytotic sites in the plasma membrane of cells expressing GFP-SNAP-25 constructs.

Fluorescence was visualized using an Olympus Fluoview FV300 confocal laser system mounted in a IX-71 inverted microscope incorporating a 100X UPlanSApo oil-immersion objective. This system allows for z axis reconstruction with theoretical z slices about 0.5 μm thick, and sequential mode studies in double labeling experiments.

Total internal reflection fluorescence microscopy (TIRFM) studies of GFP and DsRed-SNAP-25 dynamics, vesicular motion and fusion.

A through-the-lens TIRFM system was configured using the Olympus IX-71 inverted microscope indicated above with a 60x PlanApo 1.45 N.A. Olympus TIRFM objective. Epifluorescence and laser illumination (488 nm argon ion 40 mW or 543 nm He/Ne 10 mW: Melles Griot, Carlsbad, CA, USA) was selected using an Olympus TIRFM IX2-RFAEVA combiner system, modifying the angle of laser incidence. Fluorescence emission was split using an Optosplit II system (Cairn Research Ltd, Faversham, UK) equipped with GFP and rhodamine filter sets. The separated images were simultaneously acquired at 20 ms per frame using an Electron Multiplier CCD cooled camera (C9100-02 model, Hamamatsu photonics, Japan) and stored in an IBM compatible PC. TIRFM calibration was performed using 100 nm fluorescent beads (Molecular Probes, Invitrogen detecting technologies, Carlsbad, CA, USA). The fluorescence intensities were

determined at different vertical planes with step lengths of 100 nm using the motorized system mounted on the microscope and the image was obtained for both epifluorescence and TIRFM. The depth of penetration for the evanescent field was estimated as ~200 nm (1/e depth of 180 ± 16 nm) mainly permitting the visualization of the static beads adhered to the coverslip. In contrast, beads in suspension undergoing random movement were infrequently seen in TIRFM and the vast majority was visualized by epifluorescence. Vesicle labeling was performed using either 1 μM lysotracker red [24] in experiments aimed at studying the motion of granules colocalized with GFP-SNAP-25 patches or for 15 min with 2 μM acridine orange in experiments studying vesicle fusion. In the latter, the granules were assessed by the red acridine orange fluorescence in mature acidic vesicles whereas their fusion was followed by the green flashes produced after matrix neutralization during exocytosis. In these experiments laser intensity was the lowest permitting vesicle visualization in order to avoid light induced granule lysis or exocytosis [41]. Experiments with individual cells were discarded if fusion events were observed during the initial incubation with basal buffer.

Images were processed using the ImageJ program with Plugins for: particle centroid tracking, ROI measurements, image average, multiple channel image comparison, and co-localization analysis [42]. Further analysis such as the MSD determinations according to Qian et al. 1991 [22] and z distances according to John et al. 2001 [29] were performed using home made macros for Igor Pro (WaveMetrics Inc, Lake Oswego, OR, USA). For the analysis of fusion events in acridine orange labeled vesicles, the green channel images taken at 20 ms intervals that showed fusion flashes were subjected to maximal intensity determination (see Figure 7) and transferred to Igor Pro. Fusion events were analyzed using software developed for amperometric detection of exocytotic events (Quanta analysis, [43]. Kinetic parameters such the time at the half height amplitude ($t_{1/2}$) were obtained for hundreds of fusion events and they were represented as distributions. The fusion peak shape was averaged for individual cells and studied for statistical variations. Graphics were obtained with IgorPro, Graphpad Prism (GraphPad software, San Diego, CA, USA) and Adobe Photoshop 7.0.

Acknowledgements.

We thank Dr Juan Lerma for the critical reading of the manuscript and Dr Joan Blasi for kindly providing the BoNT A light chain vector. This work was supported by grants from the Spanish Ministry of Education and Culture (MEC, Fondos FEDER: BFU2005-02154/BFI), and the Generalitat Valenciana (GRUPOS 03/040 and ACOMP06/036). IL was recipient of a fellowship from the MEC of Spain.

References

1. Bennett MK, Scheller RH. The molecular machinery for secretion is conserved from yeast to neurons. *Proc Natl Acad Sci U S A* **1993**; 90**:** 2559-2563.

2. Bennett MK, Calakos N, Kreiner T, Scheller RH. Synaptic vesicle membrane proteins interact to form a multimeric complex. *J Cell Biol* **1992**; 116**:** 761-775.

3. Sollner T, Bennett MK, Whiteheart SW, Scheller RH, Rothman JE. A protein assembly-disassembly pathway in vitro that may correspond to sequential steps of

synaptic vesicle docking, activation, and fusion. *Cell* **1993**; 75**:** 409-418.

4. Sudhof TC. The synaptic vesicle cycle revisited. *Neuron* **2000**; 28**:** 317-320.

5. Oyler GA, Higgins GA, Hart RA et al. The identification of a novel synaptosomal-associated protein, SNAP-25, differentially expressed by neuronal subpopulations. *J Cell Biol* **1989**; 109**:** 3039-3052.

6. Trimble WS. Analysis of the structure and expression of the VAMP family of synaptic vesicle proteins. *J Physiol Paris* **1993**; 87**:** 107-115.

7. Weber T, Zemelman BV, McNew JA et al. SNAREpins: minimal machinery for membrane fusion. *Cell* **1998**; 92**:** 759-772.

8. Montecucco C, Schiavo G. Mechanism of action of tetanus and botulinum neurotoxins. *Mol Microbiol* **1994**; 13**:** 1-8.

9. Criado M, Gil A, Viniegra S, Gutierrez LM. A single amino acid near the C terminus of the synaptosomeassociated protein of 25 kDa (SNAP-25) is essential for exocytosis in chromaffin cells. *Proc Natl Acad Sci U S A* **1999**; 96**:** 7256-7261.

10. Xu T, Rammner B, Margittai M, Artalejo AR, Neher E, Jahn R. Inhibition of SNARE complex assembly differentially affects kinetic components of exocytosis. *Cell* **1999**; 99**:** 713-722.

11. Wei S, Xu T, Ashery U et al. Exocytotic mechanism studied by truncated and zero layer mutants of the C-terminus of SNAP-25. *EMBO J* **2000**; 19**:** 1279-1289.

12. Sorensen JB, Matti U, Wei SH et al. The SNARE protein SNAP-25 is linked to fast calcium triggering of exocytosis. *Proc Natl Acad Sci U S A* **2002**; 99**:** 1627-1632.

13. Rettig J, Neher E. Emerging roles of presynaptic proteins in Ca++-triggered exocytosis. *Science* **2002**; 298**:** 781-785.

14. Rickman C, Meunier FA, Binz T, Davletov B. High affinity interaction of syntaxin and SNAP-25 on the plasma membrane is abolished by botulinum toxin E. *J Biol Chem* **2004**; 279**:** 644-651.

15. An SJ, Almers W. Tracking SNARE complex formation in live endocrine cells. *Science* **2004**; 306**:** 1042-1046.

16. Lopez I, Giner D, Ruiz-Nuno A et al. Tight coupling of the t-SNARE and calcium channel microdomains in adrenomedullary slices and not in cultured chromaffin cells. *Cell Calcium* **2007**; 41**:** 547-558.

17. Oheim M, Loerke D, Stuhmer W, Chow RH. The last few milliseconds in the life of a secretory granule. Docking, dynamics and fusion visualized by total internal reflection fluorescence microscopy (TIRFM). *Eur Biophys J* **1998**; 27**:** 83-98.

18. Steyer JA, Horstmann H, Almers W. Transport, docking and exocytosis of single secretory granules in live chromaffin cells. *Nature* **1997**; 388**:** 474-478.

19. Bark IC, Wilson MC. Human cDNA clones encoding two different isoforms of the nerve terminal protein SNAP-25. *Gene* **1994**; 139**:** 291-292.

20. Hayashi T, McMahon H, Yamasaki S et al. Synaptic vesicle membrane fusion complex: action of clostridial neurotoxins

on assembly. *EMBO J* **1994**; 13**:** 5051-5061.

21. Gil A, Gutierrez LM, Carrasco-Serrano C, Alonso MT, Viniegra S, Criado M. Modifications in the C terminus of the synaptosome-associated protein of 25 kDa (SNAP-25) and in the complementary region of synaptobrevin affect the final steps of exocytosis. *J Biol Chem* **2002**; 277**:** 9904-9910.

22. Qian H, Sheetz MP, Elson EL. Single particle tracking. Analysis of diffusion and flow in two-dimensional systems. *Biophys J* **1991**; 60**:** 910-921.

23. Lynch KL, Gerona RR, Larsen EC, Marcia RF, Mitchell JC, Martin TF. Synaptotagmin C2A loop 2 mediates Ca2+-dependent SNARE interactions essential for Ca2+-triggered vesicle exocytosis. *Mol Biol Cell* **2007**; 18**:** 4957-4968.

24. Becherer U, Moser T, Stuhmer W, Oheim M. Calcium regulates exocytosis at the level of single vesicles. *Nat Neurosci* **2003**; 6**:** 846-853.

25. Lang T, Bruns D, Wenzel D et al. SNAREs are concentrated in cholesterol-dependent clusters that define docking and fusion sites for exocytosis. *EMBO J* **2001**; 20**:** 2202-2213.

26. Ohara-Imaizumi M, Nishiwaki C, Kikuta T, Kumakura K, Nakamichi Y, Nagamatsu S. Site of docking and fusion of insulin secretory granules in live MIN6 beta cells analyzed by TAT-conjugated anti-syntaxin 1 antibody and total internal reflection fluorescence microscopy. *J Biol Chem* **2004**; 279**:** 8403-8408.

27. Sieber JJ, Willig KI, Kutzner C et al. Anatomy and dynamics of a supramolecular membrane protein cluster. *Science* **2007**; 317**:** 1072-1076.

28. Tsuboi T, Kikuta T, Warashina A, Terakawa S. Protein kinase C-dependent supply of secretory granules to the plasma membrane. *Biochem Biophys Res Commun* **2001**; 282**:** 621-628.

29. Johns LM, Levitan ES, Shelden EA, Holz RW, Axelrod D. Restriction of secretory granule motion near the plasma membrane of chromaffin cells. *J Cell Biol* **2001**; 153**:** 177-190.

30. Toonen RF, Kochubey O, de WH et al. Dissecting docking and tethering of secretory vesicles at the target membrane. *EMBO J* **2006**; 25**:** 3725-3737.

31. Nofal S, Becherer U, Hof D, Matti U, Rettig J. Primed vesicles can be distinguished from docked vesicles by analyzing their mobility. *J Neurosci* **2007**; 27**:** 1386-1395.

32. Xu T, Binz T, Niemann H, Neher E. Multiple kinetic components of exocytosis distinguished by neurotoxin sensitivity. *Nat Neurosci* **1998**; 1**:** 192-200.

33. Graham ME, Washbourne P, Wilson MC, Burgoyne RD. Molecular analysis of SNAP-25 function in exocytosis. *Ann N Y Acad Sci* **2002**; 971**:** 210-221.

34. Gutierrez LM, Viniegra S, Rueda J, Ferrer-Montiel AV, Canaves JM, Montal M. A peptide that mimics the C-terminal sequence of SNAP-25 inhibits secretory vesicle docking in chromaffin cells. *J Biol Chem* **1997**; 272**:** 2634-2639.

35. Cormack BP, Valdivia RH, Falkow S. FACS-optimized mutants of the green fluorescent protein (GFP). *Gene* **1996**; 173**:** 33-38.

36. Geller AI, During MJ, Haycock JW, Freese A, Neve R. Long-term increases in neurotransmitter release from neuronal cells expressing a constitutively active adenylate cyclase from a herpes simplex virus type 1 vector. *Proc Natl Acad Sci U S A* **1993**; 90**:** 7603-7607.

37. Lim F, Hartley D, Starr P et al. Generation of high-titer defective HSV-1 vectors using an IE 2 deletion mutant and quantitative study of expression in cultured cortical cells. *Biotechniques* **1996**; 20**:** 460-469.

38. Aguado F, Gombau, L, Majó G, Marsal J, Blanco J, Blasí, J. Regulated secretion is inpaired in AtT-20 endocrine cells stably transfected with Botulinum Neurotoxin A light chain. *J. Biol. Chem.* **1997**; 272: 26005-26008.

39. Aunis D, Guerold B, Bader MF, Cieselski-Treska J. Immunocytochemical and biochemical demonstration of contractile proteins in chromaffin cells in culture. *Neuroscience* **1980**; 5**:** 2261-2277.

40. Lazarides E. Actin, alpha-actinin, and tropomyosin interaction in the structural organization of actin filaments in nonmuscle cells. *J Cell Biol* **1976**; 68**:** 202-219.

41. Henkel AW, Upmann I, Bartl CR et al. Light-induced exocytosis in cell development and differentiation. *J Cell Biochem* **2006**; 97**:** 1393-1406.

42. Neco P, Giner D, Viniegra S, Borges R, Villarroel A, Gutierrez LM. New roles of myosin II during vesicle transport and fusion in chromaffin cells. *J Biol Chem* **2004**; 279**:** 27450-27457.

43. Mosharov EV, Sulzer D. Analysis of exocytotic events recorded by amperometry. *Nat Methods* **2005**; 2**:** 651-658.

FIGURE LEGENTS

Fig. 1. GFP-SNAP-25 form clusters in the plasma membrane of cultured bovine chromaffin cells.

Cultured chromaffin cells were infected with the expression vectors for GFP-SNAP-25 and GFP-SNAP-25 Δ9 and after 2 days, fluorescence was studied using TIRFM. Panels A and B show representative images of the round clusters formed by the wild type and truncated Δ9 GFP-SNAP-25, respectively. Microdomains formed by both constructs were similar in area as demonstrated in the distribution size analysis of panel C. The mean average size correspond to 0.26 ± 0.02 and 0.25 ± 0.02 ± 0.02 μm^2 for GFP-SNAP-25 (n=71 clusters) and the Δ9 constructs (n=75 clusters), respectively. Bars represent 5 μm.

Fig. 2. GFP-SNAP-25 clusters colocalize with syntaxin-1 and synaptobrevin 2.

Chromaffin cells expressing GFP-SNAP-25 were fixed and permeabilized as indicate in the Methods. The cells were then incubated with a chicken anti-syntaxin 1 antibody which was visualized with a rhodamine coupled secondary antibody. A TIRFM image of the GFP-SNAP-25 microdomains is shown (A), as well as syntaxin-1 immunolocalization (B) and a superposition of the images from both channels showing the colocalized pixels in yellow (C). The colocalization mask displays the pixels with more than 50 % of the intensity in both channels (D). In other experiments cells were co-infected with amplicons containing GFP-synaptobrevin (E) and DsRed-SNAP-25 (F) vectors and the cellular fluorescence was visualized by TIRFM. Colocalization was seen in the merged images (G) and in the corresponding colocalization mask (H). Bars represent 2 μm.

Fig. 3. SNARE microdomain movement is enhanced in cells expressing the truncated GFP-SNAP-25 Δ9.

The dynamics of the microdomains formed by GFP-SNAP-25 constructs were studied in time-lapse images taken at 1 s intervals. Panels A and B show images separated by 7 seconds intervals of several clusters in cells expressing GFP-SNAP-25 (A) and GFP-SNAP-25 Δ9 (B). The microdomains marked with the cross display lateral mobility in the XY plane which was studied by measuring the centroid coordinates (C), the pathways corresponding to the movements over 30 s showed the restricted movement characteristic of the cells expressing the wild type isoform, as well as the enhancement of XY mobility for the clusters containing the truncated form (C). The variations in the intensity of fluorescence indicate the different mobility in the Z plane for the same patches (panel D).

Fig. 4. Lateral cluster movement is altered in cells expressing the truncated GFP-SNAP-25 Δ9.

The displacement of the centroids corresponding to 80 microdomains from at least 10 cells was studied in cells expressing wild type and Δ9 GFP-SNAP-25 over 20 s periods. The calculated speeds were binned at 2 nm/s intervals and plotted as a distribution (panel A). The average speed was 22 ± 1 and 36 ± 2 nm/s for microdomains in cells expressing the wild type and Δ9 constructs, respectively. In a different analysis, the centroid coordinates were used to calculate the mean square displacement (MSD) at different time intervals (panel B). From the

slope of the curves, the value of the apparent diffusion coefficient was derived (slope=4*D, 29), corresponding to the mobility of GFP-SNAP-25 (4.6 $\pm$ 0.1 x10^{-5} μm^2/s, n=74), and GFP-SNAP-25 Δ 9 patches (10.2 $\pm$ 0.1 x10^{-5} μm^2/s, n=99).

Fig. 5. SNARE cluster movement perpendicular to the plasma membrane increases in cells expressing GFP-SNAP-25 Δ9.

The motion of the GFP-SNAP-25 microdomains in the Z plane was investigated following the time course of fluorescence intensity. The intensity of the maximal fluorescence corrected for background intensity was obtained for individual clusters and transformed into Z distances using the exponential decay characteristic of the evanescent field. The distances obtained were plotted against experimental time. **A** Examples of z distance calculations for representative clusters formed by both wild type and Δ9 constructs are shown. **B**. The calculation of the fraction of time spent by GFP-SNAP-25 (4514 z distances from 74 patches, mean distance 128 ± 9 nm), and GFP-SNAP-25 Δ9 patches (4392 z distances from 72 clusters, mean distance 198 ± 14 nm) at different distances from the evanescent field origin and binned at 20 nm intervals. C. Distribution of the range of distances (Δz) covered during in 60 s observation periods by the SNARE microdomains analyzed above. D. The mean Δz value obtained for GFP-SNAP-25 (107 ± 7 nm, n=74) and GFP-SNAP-25 Δ9 (150 ± 9 nm, n=72) were statistically different ($p<0.005$ using the student t-test).

Fig. 6. High intracellular calcium reduces SNARE cluster motion in cells expressing GFP-SNAP-25 Δ9.

Cluster motion was studied in cells expressing GFP-SNAP-25 Δ9 before and after incubation of the cells with K/H containing 10 mM $CaCl_2$ and 5 μM ionomycin during 5 min. Depicted are frames separated by 10 s intervals showing the motion of different microdomains before (A) and after (B) the elevation of intracellular calcium. In A and B a cross was used to better apreciation of cluster movements. The displacement of the centroids corresponding to 79 microdomains from 30 cells was studied over 20 s periods before and after the treatment. The calculated speeds were binned at 2 nm/s intervals and plotted as a distribution (C). The average speed was 36 ± 1 (before) and 25 ± 1 nm/s (after) . Panel D depits the mean square displacement (MSD) at different time intervals in both experimental conditions. From the slope of the curves, the value of the apparent diffusion coefficient was calculated to be 12.1 $\pm$ 0.3 x10^{-5} μm^2/s (before), and 4.3 $\pm$ 0.1 x10^{-5} μm^2/s (after high Ca^{2+} and ionomycin addition). Panels E and F. As a control the same experiments were performed with 65 clusters in 22 cells were full length GFP-SNAP-25 was expressed. In this case the dynamic parameters changed from 24 $\pm$ 2 nm/s (before)) to 28 $\pm$ 2 nm/s and from 4.1 $\pm$ 0.1 x10^{-5} to 3.7 $\pm$ 0.2 x10^{-5} μm^2/s, respectively. Bars represent 1 μm.

Fig. 7. The movement of the vesicles colocalizing with SNARE patches correlates with the dynamics of the clusters.

Vesicle movement was studied in cells expressing GFP-SNAP-25 constructs using lysotracker red labeling as indicated in the Methods. TIRFM experiments commenced by visualizing the SNARE patches (A panel for wild type and E panel for the truncated Δ9 form) and vesicles (B and F) to assess the colocalization through image merging (C and G) and to calculate the 50 % intensity colocalization mask (D and H). Bars represent 2 μm. **I.** The

distribution of speeds in vesicles colocalizing with GFP-SNAP-25 (mean speed of 23 ± 1 nm/s, n=73 vesicles) or GFP-SNAP-25 Δ9 patches (mean of 30 ± 1 nm/s, n=57 vesicles). J. Mean square displacement vs time for the vesicles colocalizing with the wild type (coefficient of diffusion of 3.7 $\pm$ 0.2 x10^{-5} μm^2/s), or Δ 9 form of SNAP-25 (coefficient of diffusion of 15.0 $\pm$ 0.3 x10^{-5} μm^2/s). **K.** Distribution of the Z distances corresponding to the vesicles colocalizing with GFP-SNAP-25 (mean distance of 122 ± 9 nm, n=73 vesicles) or the Δ9 patches (mean distance of 199 ± 13 nm, n=57 vesicles). **L.** Calculation of the mean range of z displacement (ΔZ) obtained for vesicles colocalizing with GFP-SNAP-25 (mean value of 84 ± 6 nm), and GFP-SNAP-25 Δ9 microdomains (mean of 104 ± 8 nm/s).

Fig. 8. Low fusion probability of vesicles associated with high mobility SNAP-25 Δ9 clusters.
Cells expressing DsRed-SNAP-25 constructs were incubated with acridine orange as indicated in the methods and then stimulated with a high potassium solution (59 mM KCl) for 1 min. During stimulation, TIRFM images of the red channel showed SNARE clusters and vesicles (DsRed and the red component of acridine orange) and the green channel showed fusion events (green fluorescence of acridine orange when the vesicle interior is neutralized during exocytosis), acquired simultaneously at 20 ms intervals using an image splitter with the appropriate filters. Panels A and B depict four images of both channels taken at 10 s intervals from cells expressing the wild type form of SNAP-25 (**A**) or the truncated form SNAP-25 Δ9 (**B**) in a representative experiment. Panels **C** and **D**, show the accumulative sum of the images from both experiments, depicting vesicles and SNAREs as red spots and fusion events as green flashes. These images demonstrate the higher probability of vesicle fusion in cells expressing the wild type form of SNAP-25 (**C**) when compared with the vesicles in cells where the truncated form is expressed (**D**). These accumulative images were used to estimate the probability of fusion during a 60 s depolarization (**E**). **F**. In cells expressing SNAP-25 Δ9 , the probability of fusion was estimated for vesicles presenting low motion (less than 2 diameters motion in 20 S, immobile vesicles) and highly mobile vesicles (mobile vesicles). **G**. The maximum fluorescence in the green channel images taken at 20 ms intervals was used to obtain the secretory activity profiles of these cells expressing SNAP-25 isoforms. Bars represent 2 μm.

Fig. 9. Fusion events are slower in cells expressing highly mobile SNARE clusters.
Fusion kinetics was analyzed in the experiments described in the previous figure. Exocytosis was simultaneously detected as the disappearance of vesicles in the red channel (panel A for SNAP-25 wild type expressing cells and C for cells expressing the Δ9 form) or the generation of a green flash product of acridine orange neutralization during fusion (panels B and D, respectively). E. The plots of the maximal fluorescence of the green channels vs time depict the kinetics of the fusion events as spikes for the examples in the previous panels. The analysis of events in cells expressing full length SNAP-25 and cells expressing the truncated form gave average spikes representative of the individual cells presented in panel F. Panel G shows the distribution of $t_{1/2}$ values corresponding to 370 events in 22 SNAP-25 expressing cells and 342 fusions in 29 cells expressing SNAP-25 Δ9. Average $t_{1/2}$ values of 178 ± 7 ms and 218 ± 9 were obtained for these cells, respectively.

Figure 1

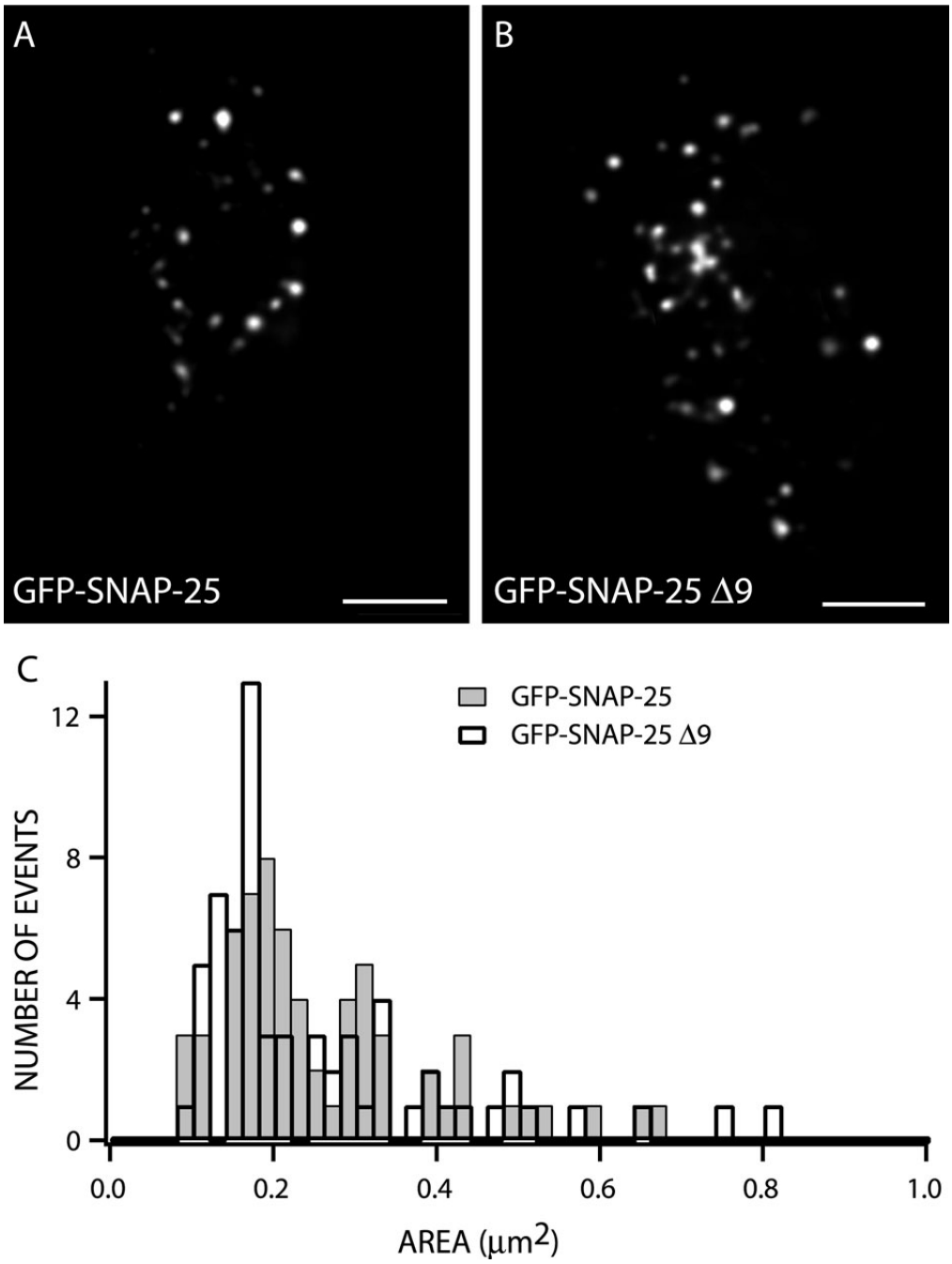
A
GFP-SNAP-25
B
GFP-SNAP-25 Δ9
C
GFP-SNAP-25
GFP-SNAP-25 Δ9
NUMBER OF EVENTS
0
4
8
12
0.0
0.2
0.4
0.6
0.8
1.0
AREA (μm2)

Figure 2

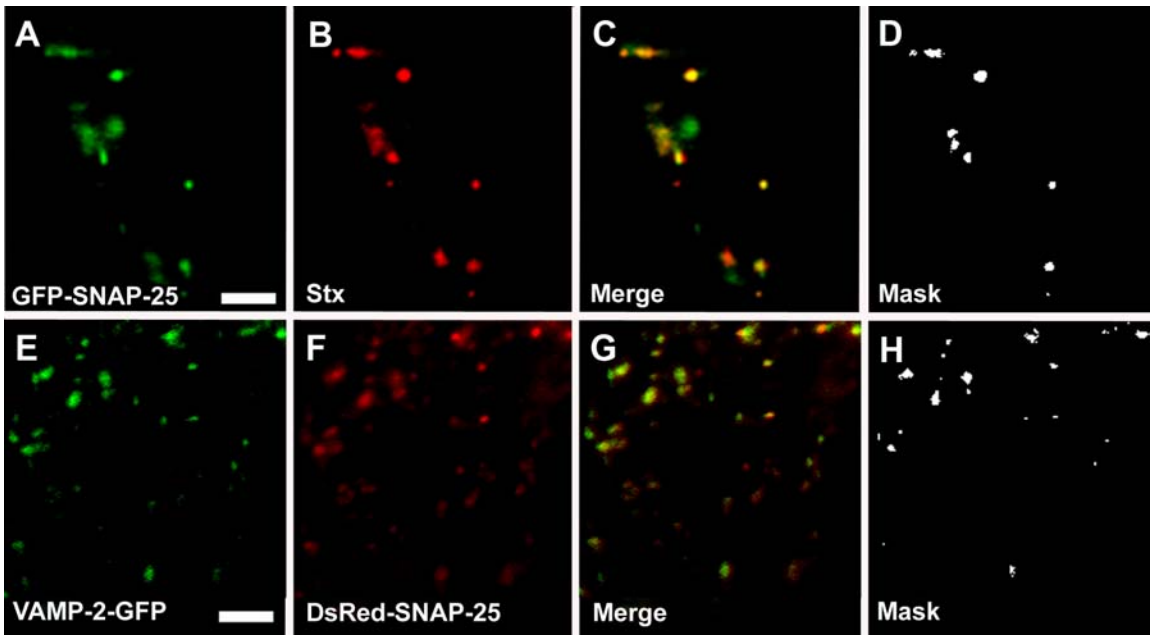
A
GFP-SNAP-25
B
Stx
C
Merge
D
Mask
E
VAMP-2-GFP
F
DsRed-SNAP-25
G
Merge
H
Mask

Figure 3.

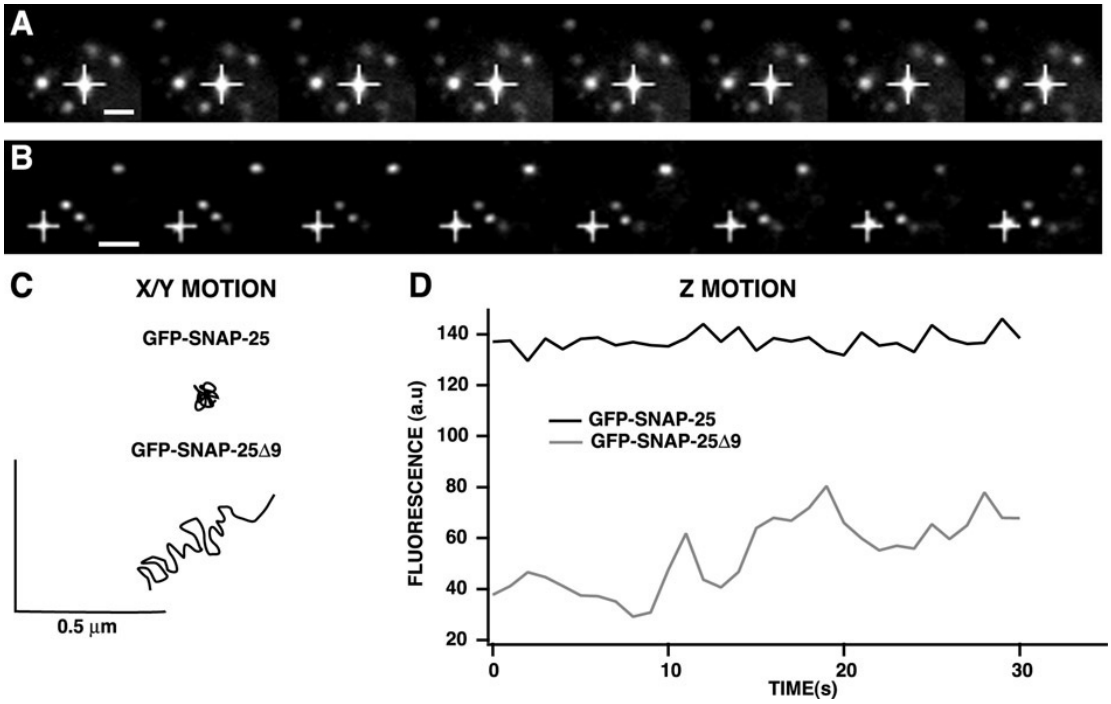
A
B
C
X/Y MOTION
GFP-SNAP-25
GFP-SNAP-25Δ9
0.5 μm
D
Z MOTION
FLUORESCENCE (a.u)
140
120
100
80
60
40
20
GFP-SNAP-25
GFP-SNAP-25Δ9
0
10
20
30
TIME(s)

Figure 4.

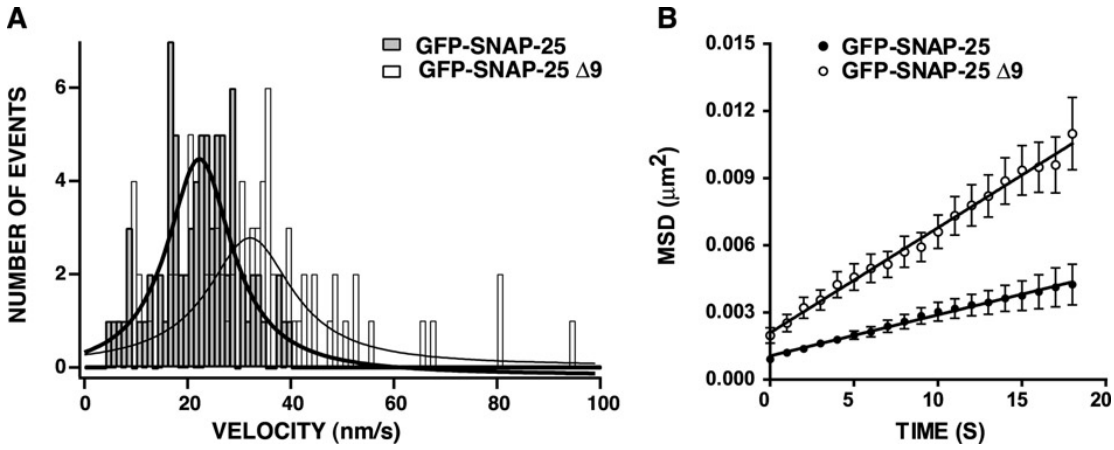
A
GFP-SNAP-25
GFP-SNAP-25 Δ9
NUMBER OF EVENTS
VELOCITY (nm/s)
B
GFP-SNAP-25
GFP-SNAP-25 Δ9
MSD (μm2)
TIME (S)

Figure 5.

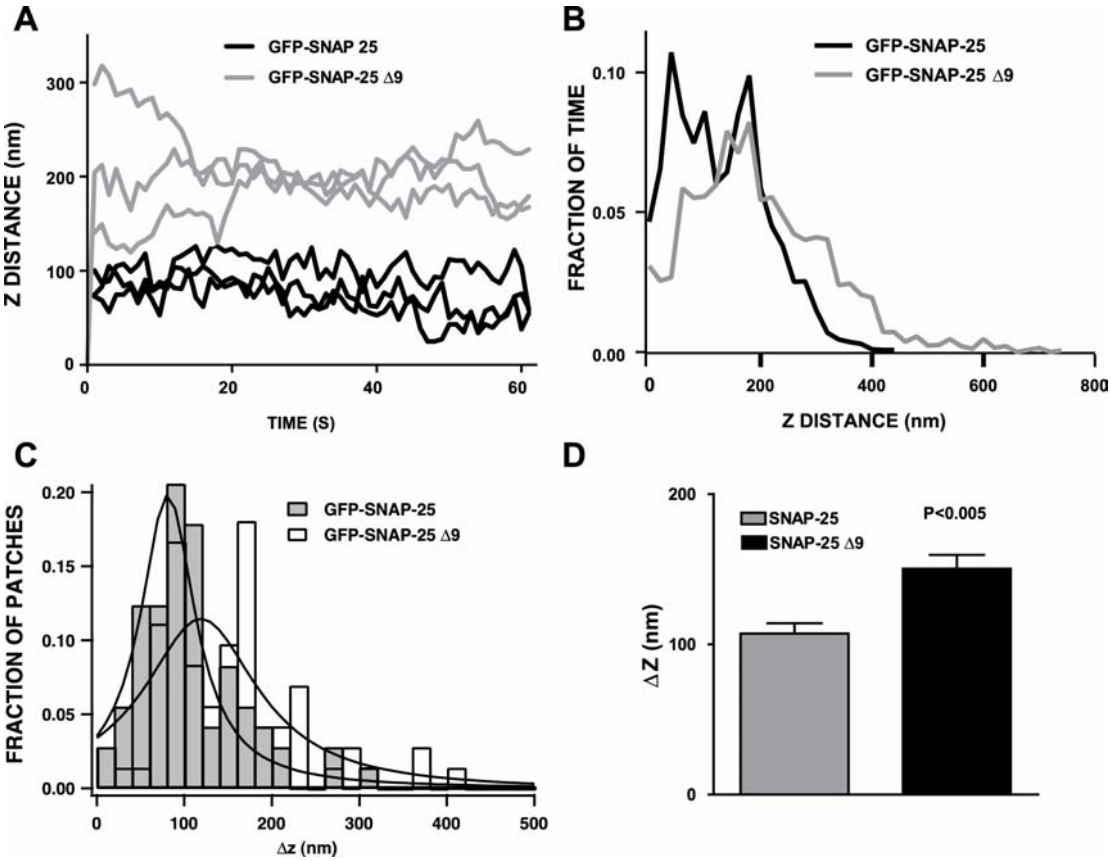
A
GFP-SNAP 25
GFP-SNAP-25 Δ9
Z DISTANCE (nm)
TIME (S)
B
GFP-SNAP-25
GFP-SNAP-25 Δ9
FRACTION OF TIME
Z DISTANCE (nm)
C
GFP-SNAP-25
GFP-SNAP-25 Δ9
FRACTION OF PATCHES
Δz (nm)
D
SNAP-25
SNAP-25 Δ9
P<0.005
ΔZ (nm)

Figure 6.

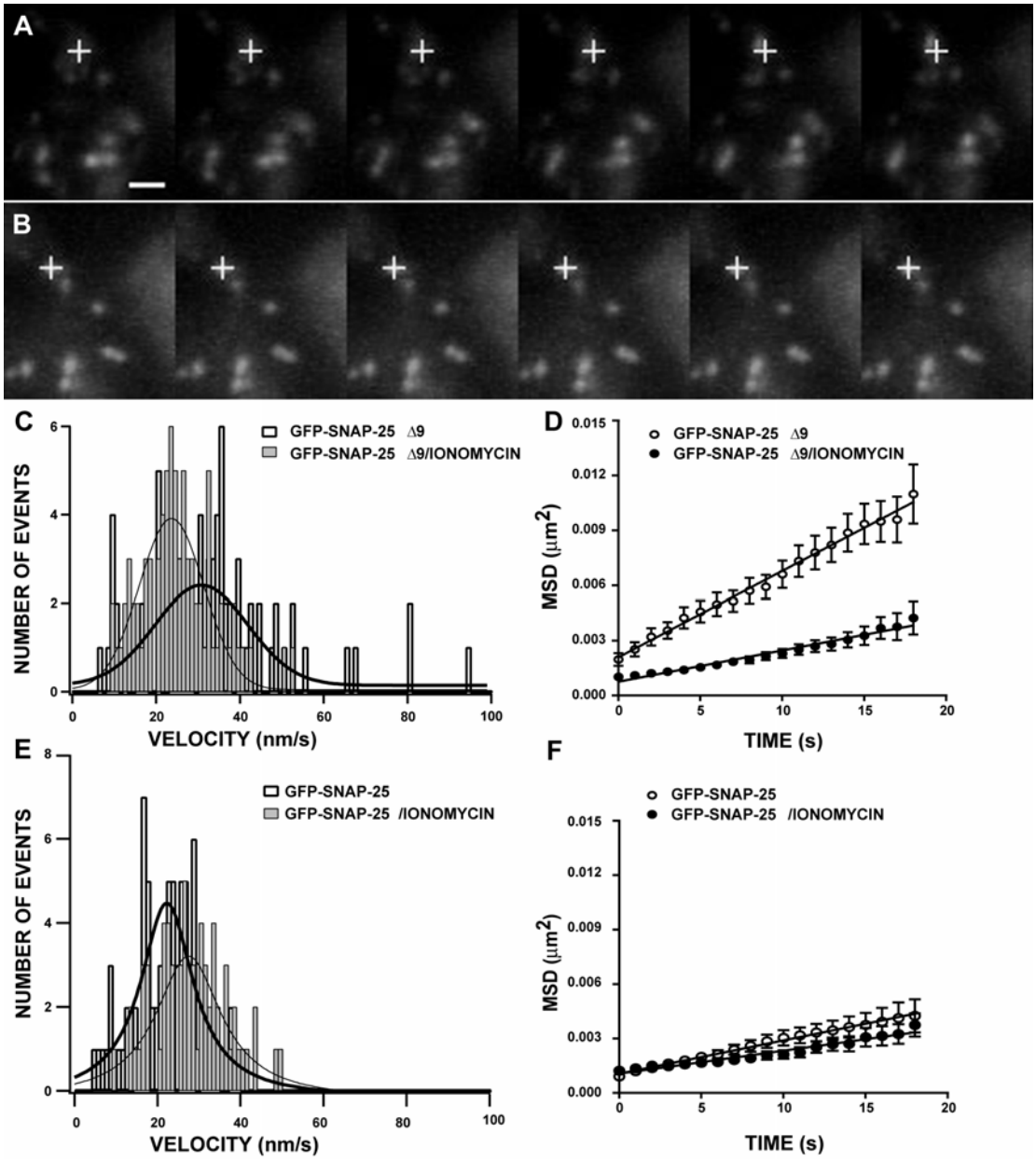
A
B
C
GFP-SNAP-25 Δ9
GFP-SNAP-25 Δ9/IONOMYCIN
NUMBER OF EVENTS
VELOCITY (nm/s)
D
GFP-SNAP-25 Δ9
GFP-SNAP-25 Δ9/IONOMYCIN
MSD (μm2)
TIME (s)
E
GFP-SNAP-25
GFP-SNAP-25 /IONOMYCIN
NUMBER OF EVENTS
VELOCITY (nm/s)
F
GFP-SNAP-25
GFP-SNAP-25 /IONOMYCIN
MSD (μm2)
TIME (s)

Figure 7.

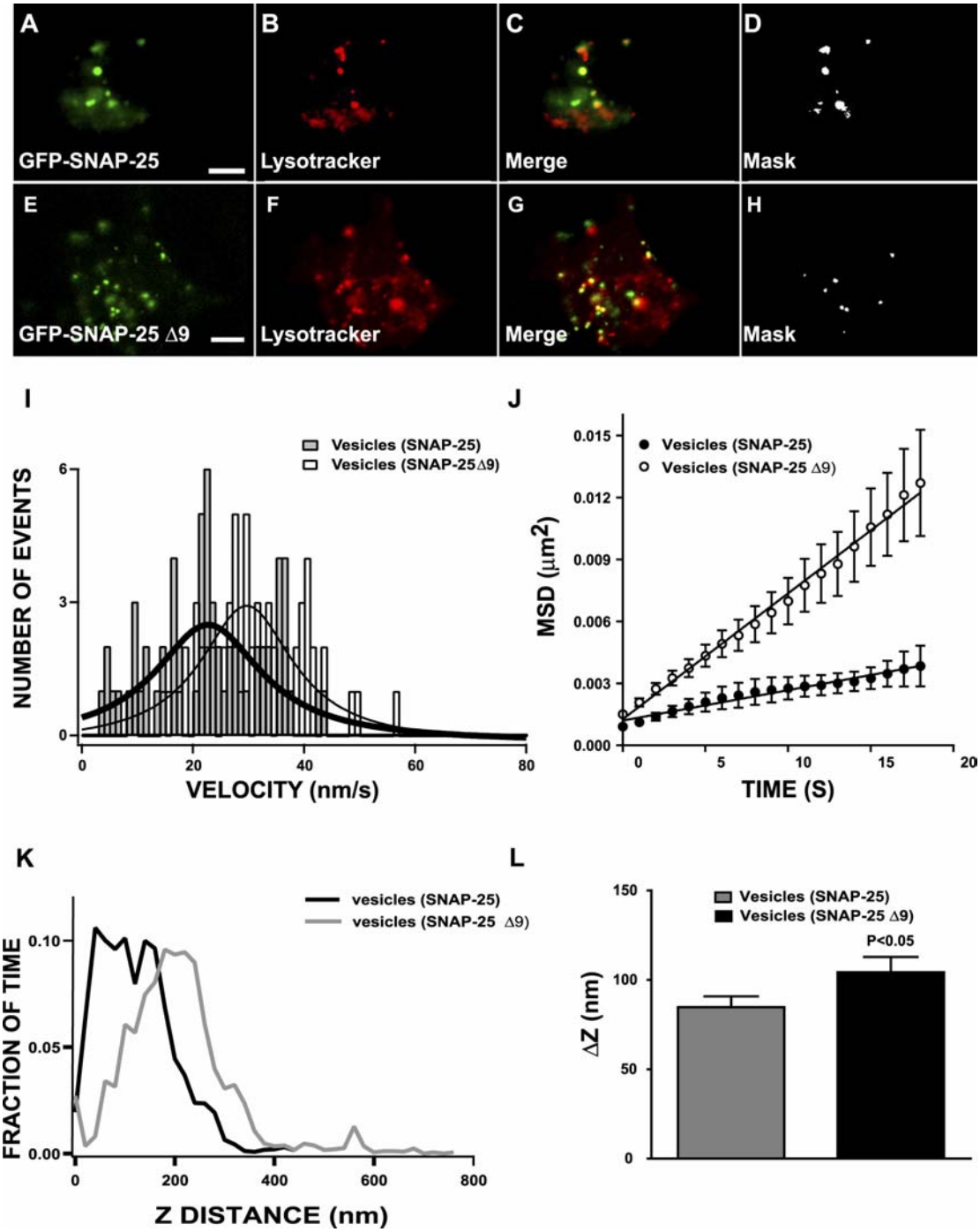
A
GFP-SNAP-25
B
Lysotracker
C
Merge
D
Mask
E
GFP-SNAP-25 Δ9
F
Lysotracker
G
Merge
H
Mask
I
Vesicles (SNAP-25)
Vesicles (SNAP-25Δ9)
NUMBER OF EVENTS
VELOCITY (nm/s)
J
Vesicles (SNAP-25)
Vesicles (SNAP-25 Δ9)
MSD (μm2)
TIME (S)
K
vesicles (SNAP-25)
vesicles (SNAP-25 Δ9)
FRACTION OF TIME
Z DISTANCE (nm)
L
Vesicles (SNAP-25)
Vesicles (SNAP-25 Δ9)
P<0.05
ΔZ (nm)

Figure 8.

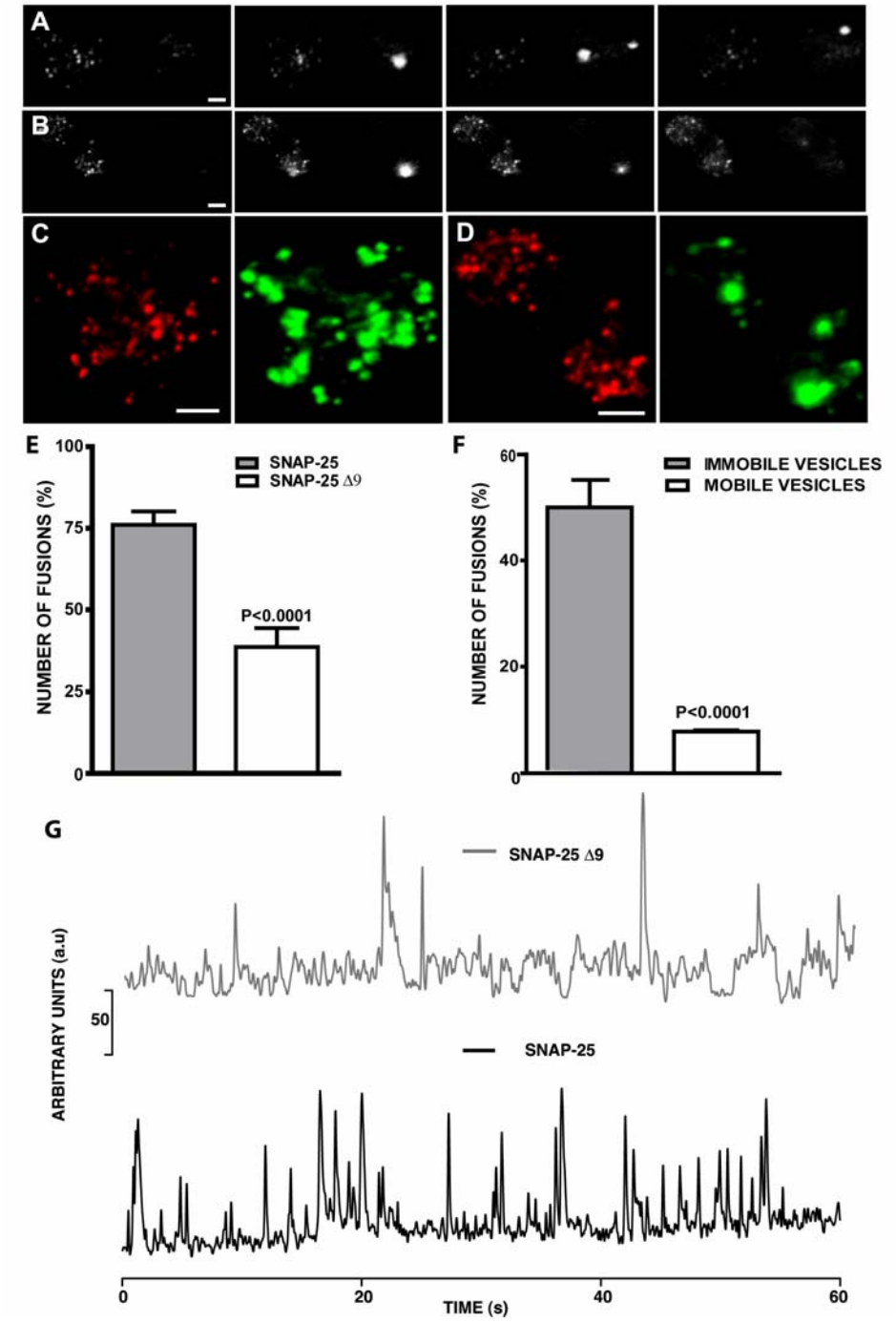
A
B
C
D
E
NUMBER OF FUSIONS (%)
100
75
50
25
0
SNAP-25
SNAP-25 Δ9
P<0.0001
F
NUMBER OF FUSIONS (%)
60
40
20
0
IMMOBILE VESICLES
MOBILE VESICLES
P<0.0001
G
ARBITRARY UNITS (a.u)
50
SNAP-25 Δ9
SNAP-25
0
20
40
60
TIME (s)

Figure 9.

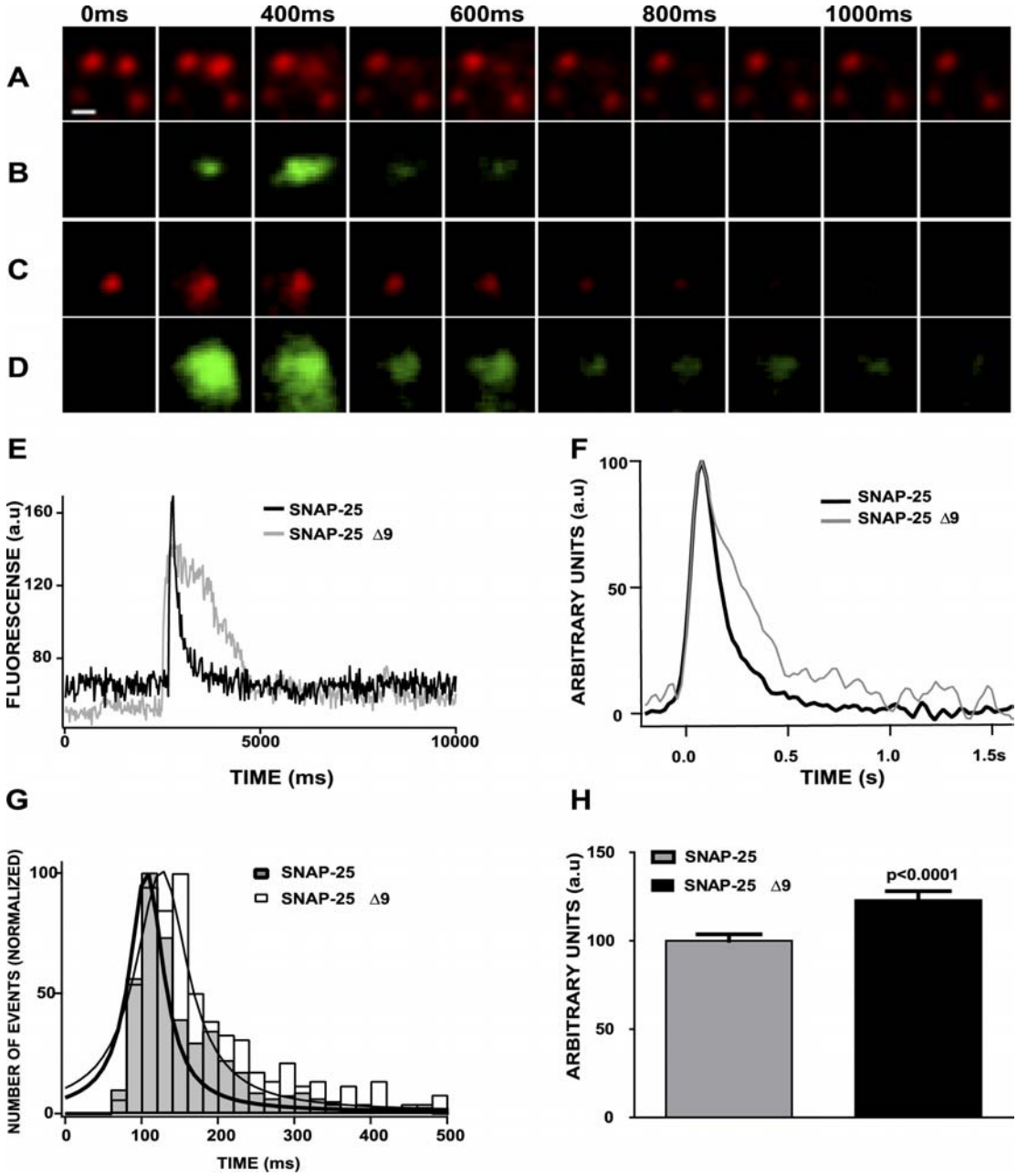
0ms
400ms
600ms
800ms
1000ms
A
B
C
D
E
FLUORESCENSE (a.u)
160
120
80
SNAP-25
SNAP-25 Δ9
0
5000
10000
TIME (ms)
F
ARBITRARY UNITS (a.u)
100
50
0
SNAP-25
SNAP-25 Δ9
0.0
0.5
1.0
1.5s
TIME (s)
G
NUMBER OF EVENTS (NORMALIZED)
100
50
0
SNAP-25
SNAP-25 Δ9
0
100
200
300
400
500
TIME (ms)
H
ARBITRARY UNITS (a.u)
150
100
50
0
SNAP-25
SNAP-25 Δ9
p<0.0001

Supplementary material

Supplementary Figure 1. GFP-SNAP-25 clusters are present in the plasma membrane of chromaffin cells. Cells infected with amplicons containing GFP-SNAP-25 sequence were stimulated by a KCl 59 mM K/H buffer and subjected to the labeling of exocytotic sites using anti-dopamine β-hydroxylase antibodies. Depicted is the green labeling of the expressed GFP-SNAP-25 protein and in red the spotted appearance of the exocytosed granule membrane stained with the antibodies coupled to rhodamine. The close location of both labelings in the periphery of the visualized cell is best observed in the insert. Bar represents 5 μm.

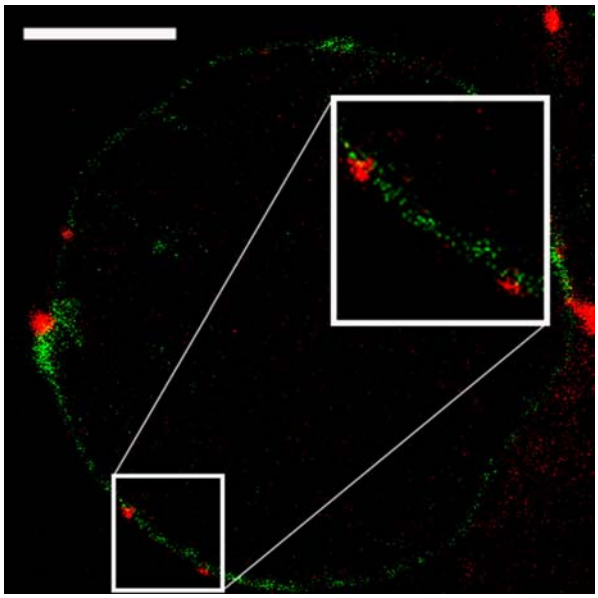

Supplementary Figure 2. Presence of the native SNAP-25 protein in the clusters formed by GFP SNAP-25 and GFP SNAP-25 Δ9 constructs. Cells infected with amplicons containing the GFP-SNAP-25 (A) and GFP-SNAP-25 Δ9 sequence (D) were stained with polyclonal anti-SNAP-25 rabbit antibodies (panels B and E in red, TRICT labelling) and visualized by confocal microscopy. The images show polar sections of the cells with the SNARE clusters clearly visible with GFP. Most of the red labeled clusters present GFP labeling and only a few present much lower GFP stain (as the indicated by arrows. Bar represents 1 μm.

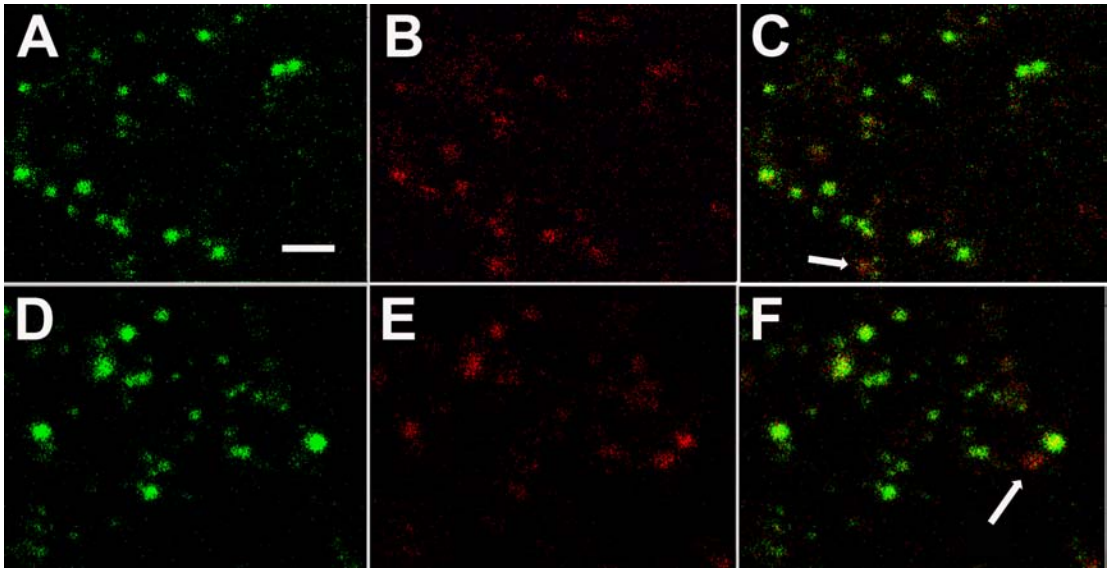

Supplementary Figure 3. Colocalization of Ds-red SNAP-25 clusters with lysotracker green labeled vesicles. Cells infected with amplicons containing the DsRed-SNAP-25 (A) and DsRed-SNAP-25 Δ9 sequence (B) were stained with lysotracker green and visualized using TIRFM. The sequences of images separated by 10 s intervals show the dynamic colocalization of green labeled granules with the relatively immobile SNARE clusters formed by wild type SNAP-25 (A) and the highly mobile microdomains formed by the truncated Δ9 form (B). Bars represent 1 μm.

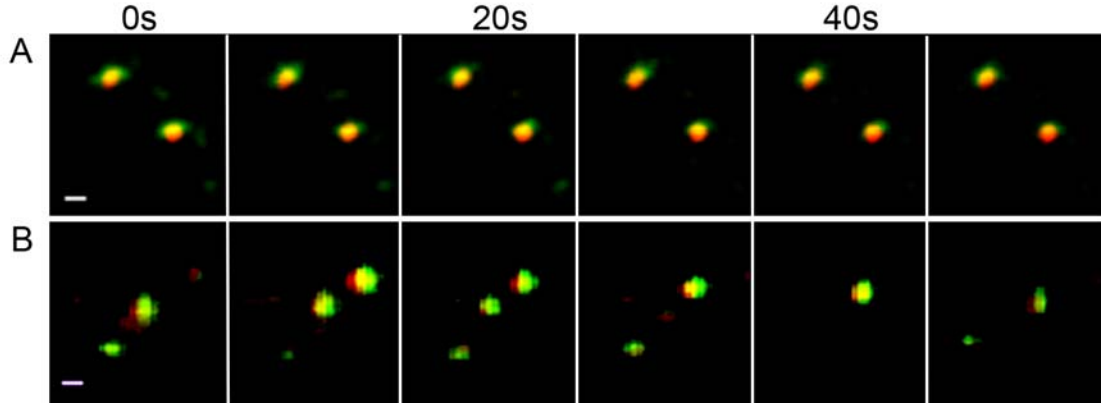

Supplementary Figure 4. Expression of the light chain of BoNT A enhances vesicle dynamics visualized with GFP-synaptobrevin in TIRFM. Chromaffin cells were transfected with GFP-synaptobrevin II in the presence of absence of a vector encoding the light chain of BoNT A. After 24 h, vesicle motion was studied by TIRFM and the averaged vesicle speed (Panel A) and MSD vs time curves (panel B) calculated for vesicles in cells

expressing GFP-synaptobrevin (CONTROL, n=56 vesicles from 7 cells) or cell expressing both GFP-synaptobrevin and the light chain of BoNT A (BoNT/A, n=72 vesicles from 9 cells). The coefficient of diffusion obtained were 7.7 $\pm$ 0.3 x10^{-5} $\mu m^2/s$ for CONTROL vesicles and 22.0 $\pm$ 0.3 x10^{-5} $\mu m^2/s$ for vesicles in cells expressing the light chain of BoNT A.

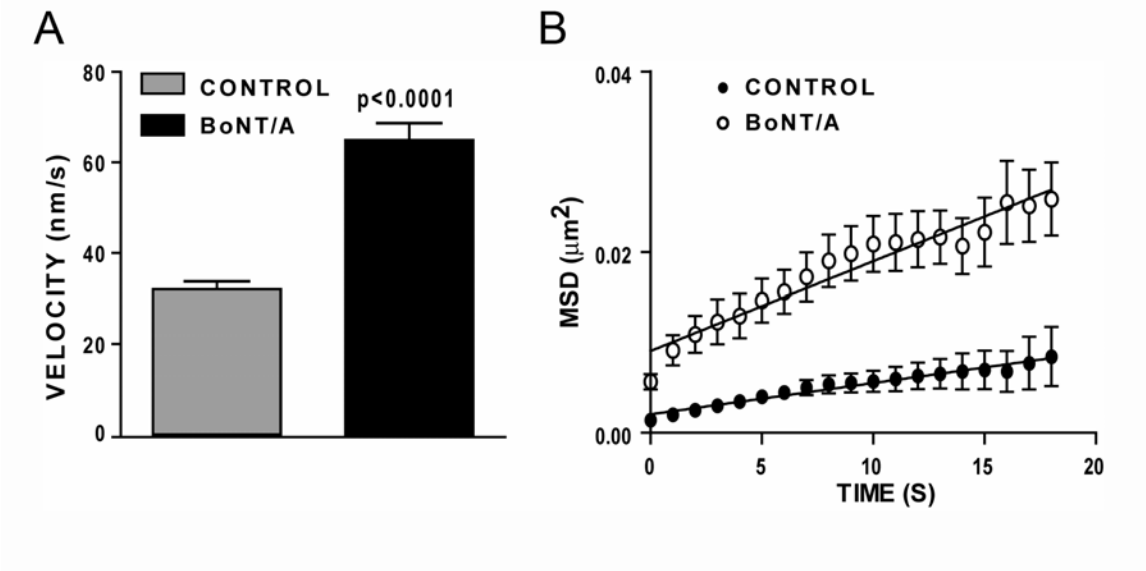

Supplementary video 1. 3D reconstruction of SNARE microdomains in a bovine chromaffin cell visualized by fluorescence confocal microscopy. Images were taken using a 100x objective and corresponded to the expression of GFP-SNAP-25 and the rodhamine inmunolabeling of syntaxin-1.

Supplementary video 2. Video of GFP-SNAP-25 microdomain dynamics visualized by TIRFM. Images were taken at 1 s intervals and corresponded to a 1 min sequence (6x times accelerated). For better appreciation of the dynamism use the repeat option of your video viewer in this and the following videos.

Supplementary video 3. Video of GFP-SNAP-25 Δ9 cluster dynamics as visualized by TIRFM. Images were taken at 1 s intervals and corresponded to a 1 min sequence (6x times accelerated).

Supplementary video 4. Exocytosis in a cell expressing DsRed-SNAP-25. Images were taken at 20 ms intervals during a 1 min cell depolarization with KCl (59 mM). The red channel (DsRed and red fluorescence from acridine orange, left side) and the green channel (right side) are visualized side by side where vesicle fusion is observed as flashes upon acridine orange neutralization during exocytosis. The video is accelerated 6x.

Supplementary video 5. Vesicle fusion in a cell expressing DsRed-SNAP-25 Δ9. Images were obtained as indicated in the previous video.